Supporting Information

Pd Doping-weakened Intermediate adsorption to Promote Electrocatalytic Nitrate Reduction on TiO_2 Nanoarrays for Ammonia Production and Energy Supply with Zinc-Nitrate Batteries

Ying Guo,[a] Rong Zhang,[a] Shaoce Zhang,[a] Yuwei Zhao,[a] Qi Yang,[a] Zhaodong Huang,[a] Binbin Dong,[b] Chunyi Zhi[a,c*]

[1]Department of Materials Science and Engineering, City University of Hong Kong, 83 Tat Chee Avenue, Kowloon, Hong Kong 999077, China

[2]National Engineering Research Center for Advanced Polymer Processing Technology， Zhengzhou University, Zhengzhou, Henan 450002, China

[3]Centre for Functional Photonics, City University of Hong Kong, Kowloon, Hong Kong

Corresponding author: Prof. Chunyi Zhi

Email: cy.zhi@cityu.edu.hk

S1. Experiment section

Chemicals

Sulfuric acid (H_2SO_4, 98%), palladium chloride ($PdCl_2$, 99.99%), deuterium oxide (D_2O, 99.9 atom % D), hydrochloric acid (HCl, 37%), lithium chloride anhydrous (LiCl, 99.0%), sodium hydroxide (NaOH, > 98%), sodium hypochlorite solution (NaClO, available chlorine 4.0 %), p-Dimethylaminobenzaldehyde ($C_9H_{11}NO$), lithium nitrate ($LiNO_3$, 99.99%), salicylic acid ($C_7H_6O_3$, 99%), ethanol (C_2H_5OH, 99.7%), hydrogen peroxide (H_2O_2, 30%), trisodium citrate ($C_6H_5Na_3O_7$, 98%), sodium nitroferricyanide dehydrate ($C_5FeN_6Na_2O{\cdot}2H_2O$, 99%), 2-propanol ($C_3H_8O$, 99.5%), titanium butoxide ($C_{16}H_{36}O_4Ti$, 99%), N-(1-naphthyl) ethylenediamine dihydrochloride ($C_{12}H_{14}N_2{\cdot}2HCl$, 98%), tetrahydrofuran (C_4H_8O, 99.5%), trimethylamine (C_3H_9N, 30 wt.% in H_2O), and 1-butyl-3-methylimidazolium chloride ($C_8H_{15}ClN_2$, 97%) were purchased from Shanghai Macklin Biochemical Co., Ltd. Nitric acid (65%) was purchased from Sigma-Aldrich. Ar gas (99.999 % purity) were supplied by Linde HKO Ltd. W1S1005 carbon cloth was purchased from Fuel Cell Store Ltd.

Synthesis of TiO_2 array on CC

The CC-supported TiO_2 array was prepared by a seed-assisted approach. Typically, the CC (3 cm×5 cm) was pre-treated by acetone and ethanol several times and then dried at room temperature. The dried CC was immersed in 2-propanol solution containing 0.075 M titanium butoxide and tried in an oven at 60°C for 3 times. Then, the CC was subjected to heat treatment in air at 500°C for 30 min to form TiO_2 seeds. Subsequently,

the TiO_2 seed decorated CC was placed into a Teflon-lined stainless-steel autoclave (80 mL) which contains 30 mL 2-propanol, 30 mL concentrated HCl, and 1.32 mL titanium butoxide, and then the stainless steel autoclave was transferred to an oven at 150°C for 6 h. when autoclave was cooled down to room temperature, the CC was removed from it and rinsed with distilled water several times and dried. The $Ti(OH)_2Cl_2(OH)_2$ precursor nanoarray on CC was obtained. Finally, the precursor array was annealed at 550°C under ambient conditions for 4 hours to form TiO_2 array on CC with the loading mass of around 10 mg/cm^2.

Synthesis of Pd/TiO_2 array on CC

Pd/TiO_2 array was prepared by ion exchange between Pd^{2+} and H^+. Typically, 3 cm×5 cm $Ti(OH)_2Cl_2(OH)_2$ precursor array was transferred into a Teflon-lined stainless steel autoclave (80 mL) which contains 10 mM $PdCl_2$ and 20 mM HCl. Then the autoclave was placed in an oven at 90°C for 12 h. After cooling down to room temperature, the as-obtained array was rinsed with distilled water for 3 times and annealed at 550°C for 4 hours in the Ar atmosphere. Lastly, the Pd/TiO_2 array on CC was obtained with the loading mass of around 10 mg/cm^2.

Synthesis of Pd/TiO_2 NPs

2 g of commercial TiO_2 NPs (anatase phase) was annealed at 950°C for 6 h under ambient conditions to obtain rutile TiO_2 nanoparticles. Then, 0.5 g of rutile TiO_2 NPs was placed into a Teflon-lined stainless steel autoclave (80 mL) which contains 10 mM $PdCl_2$ and 20 mM HCl. Afterward, the autoclave was transferred to an oven at 90°C for

12 h. After cooling down, Pd/TiO_2 NPs was achieved by washing TiO_2 NPs with distilled water for 3 times and annealing at 550°C for 4 hours in the Ar atmosphere.

Characterization

The crystalline, morphologies and microstructures of samples were investigated by XRD using a Bruker D2 Phaser diffractometer with Cu Kα irradiation (λ = 1.54 Å), field-emission scanning electron microscopy (FEI Quanta 450 FEG) and JEOL-2001F field-emission TEM (JEOL-2001F). The surficial chemical states and compositions of the as-obtained products were investigated by XPS (ESCALB 250) with an Al Kα X-ray beam (E = 1486.6 eV). ^{1}H-NMR measurements were performed on Bruker 600MHz ASCEND AVANCE III HD Nuclear Magnetic Resonance System (NMR-600). UV-vis spectroscopy measurements were carried out using a UV/VIS Spectrometer Lambda 2S.

Computational Details

All the computations were conducted based on the density functional theory (DFT) using the Cambridge Sequential Total Energy Package (CASTEP) code of the Masterials Studio 2018 software. The generalized gradient approximation (GGA) with the Perdew-Burke-Ernzerhof (PBE) functional were used to describe the electronic exchange and correlation effects. The kinetic-energy cutoff was set as 500 eV. The geometry optimization within the conjugate gradient method was performed with forces on each atom less than 0.05 eV/Å. An energy tolerance is 5.0×10^{-6} eV per atom, and a maximum displacement of 0.001Å was considered. A p(1 × 3) unit cell of TiO_2 (110)

surface with a two-layer model of the crystal plane was used to simulate the exposed surface of the catalysts accompanying with a sufficient vacuum gap of 15 Å. Bottom atomic Ti-O layer was fixed while other layers and the adsorbates were fully relaxed during structural optimizations. The Brillouin zone was sampled by a k-point mesh of 4 × 4 × 1.

The NO_3^- reduction reaction on the catalysts surfaces was simulated according to the following reactions (J. Am. Chem. Soc. **2020**, 142, 5702-5708.):

$*NO_3^- + H_2O + e^- \rightarrow *NO_2 + 2OH^-$

$*NO_2 + H_2O + 2e^- \rightarrow *NO + 2OH^-$

$*NO + H_2O + 2e^- \rightarrow *N + 2OH^-$

$*N + H_2O + e^- \rightarrow *NH + OH^-$

$*NH + H_2O + e^- \rightarrow *NH_2 + OH^-$

$*NH_2 + H_2O + e^- \rightarrow *NH_3 + OH^-$

Where * represent the adsorption site, the free energies for each reaction were given after correction:

$$\Delta G = \Delta E - T\Delta S$$

Where ΔE is the reaction energy obtained by the difference between reactants and products; ΔS is the change in entropy for each reaction. Entropy values are taken from the standard database in the NIST webbook (*J. Phys. Chem. Ref. Data* **1996,** 25, 551-603.). The entropies of adsorbate and adsorption site are negligible.

Electrochemical measurements

All electrochemical measurements were carried out in the Ar atmosphere. The CC-supported TiO_2 or Pd/TiO_2 (1×1 cm^2), Ag/AgCl (3 M KCl), and Pt plate (1 cm×1 cm) were used as the work electrode, the reference electrode and the counter electrode, respectively. The Pd/TiO_2 NPs modified electrode was prepared as following: first, 100 μL of Pd/TiO_2 NPs ink with 5 mg/mL of alcohol/water (v/v=1:1) solution was dropped onto a CC (1×1 cm^2); then CC with the loading mass of 0.5 mg/cm^2 was dried under ambient conditions for 2 hours. Before all electrochemical tests, a 50-cycle CV test with a scan rate of 0.1 V/s was performed to make the catalyst electrode reach the steady-state. LSV tests were conducted with the scan rate of 5 mV/s in the three-electrode system. 40 mL of the Ar-saturated electrolyte containing 1 M LiCl or 1 M LiCl + 0.25 M $LiNO_3$. The chronoamperometry tests were conducted at a series of applied potentials in a typical H-type cell that contains 40-mL electrolyte separated by a membrane (Nafion 117) on the electrochemical workstation (CHI 760E, Chenhua, China). All potentials in this work refer to RHE, E(RHE) = E(Ag/AgCl) + 0.222 + 0.059pH, where pH=7. Nafion membrane was pretreated in 5 wt% H_2O_2 aqueous solution at 80 °C for 1 h and then in ultrapure water at 80 °C for another 1 h. For isotope labeling experiments, 40-mL solution containing 0.25 M $K^{15}NO_3$+1 M LiCl was used as the NORR electrolyte. The 1-h chronoamperometry tests were conducted at the optimal potential of -0.7 V (vs RHE) in the Ar atmosphere. Then, 0.45-mL diluted electrolyte and 0.05-mL deuterium oxide (D_2O) were added into the NMR tube for further NMR (600 MHz) detection. The calibration curve was drawn by detecting the adsorption intensities of a series of $(^{15}NH_4)_2SO_4$ with the given concentration in H_2SO_4

(0.05 M) solution. Finally, the calibration curve was created by using the area integral value of two peaks. EIS measurement was carried out in an H-type cell at 1.27 V (vs Zn) in the frequency range from 0.1 Hz to 10^5 Hz with 5 mV amplitude.

Assembly of the zinc-nitrate battery and electrochemical test.

The CC-supported Pd/TiO_2 (1×1 cm^2) and Zn plate (1.5×2 cm^2) were employed as the cathode for zinc-nitrate battery. A typical H-type cell that contains 20-mL cathode electrolyte (0.25 M $LiNO_3$ + 5 M LiCl) and 20-mL anode electrolyte (5 M KOH) separated by a bipolar membrane (Nafion 117). The discharging polarization curves with a scan rate of 5 mV/s and galvanostatic tests were conducted using CHI 760E workstation and Land 2001A battery test system at room temperature, respectively. After electrochemical test, the electrolyte was diluted 5 times with distilled water, and then diluted to a certain concentration with 1 M LiCl solution for the next detection.

The power density (*P*) of zinc-nitrate battery was determined by $P = I \times V$, where *I* and *V* are the discharge current density and voltage, respectively.

The electrochemical reactions in Zn-nitrate battery are presented as following:

Cathode reaction: $NO_3^- + 7H_2O + 8e^- \rightarrow NH_4OH + 9OH^-$

Anode reaction: $4Zn + 8OH^- \rightarrow 4ZnO + 4H_2O + 8e^-$

Overall reaction: $4Zn + NO_3^- + 3H_2O \rightarrow 4ZnO + NH_4OH + OH^-$

Since cathode and anode are separated by a bipolar membrane, the electrode potentials should be calculated individually:

$$E_{cathode} = -\frac{1}{nF}\left(\Delta G_{cat} + RTln\frac{[OH^-]^9[NH_4OH]}{[NO_3^-]}\right) = 0.6\ \text{V}$$

$$E_{anode} = -\frac{1}{nF}\left(\Delta G_{ano} + RTln\frac{1}{[OH^-]^2}\right) = -1.27\ \text{V}$$

Where n, F, ΔG, R, and T are electron transfer number, the Faraday constant (96485 C/mol), standard molar Gibbs free energy change of chemical reaction at 298 K, gas constant (8.314 J/(mol K), and reaction temperature (298 K), respectively. The concentrations of $[OH^-]$ in cathode cell and anode cell are 10^{-7} and 5 mol/L, respectively. $[NO_3^-]$ is 0.25 mol/L. Assuming $[NH_4OH]$ is 10^{-3} mol/L in cathode cell. Therefore, we have $E_{overall} = E_{cathode} - E_{anode} = 1.87$ V

Determination of ammonia

The amount of the produced NH_3 was detected with the indophenol blue method. To minimize the experimental error in quantification of ammonia, all data was recorded three times to obtain the error bar. In detail, 1-mL electrolyte was taken out after NO_3RR test and diluted with 1 M LiCl, and 1.25 mL of solution containing 0.625 M NaOH, 0.36 M salicylic acid and 0.17 M sodium citrate was added. Then 150 μL sodium nitroferricyanide solution (10 mg/mL) and 75 μL NaClO (available chlorine 4.0 wt%) solution were added. After 2 h under ambient conduction, UV-Vis absorption spectrum was recorded, and the absorbance value was obtained at the wavelength of 658 nm. The standard NH_4^+ solutions with the given concentrations of $(NH_4)_2SO_4$ in 0.05 M H_2SO_4 were prepared for building the calibration curve.

Determination of hydrazine

Hydrazine in the electrolytes was also detected by the Watt-Chrisp method. A mixture of ethanol (100 mL), para(dimethylamino) benzaldehyde (2.0 g) and HCl (concentrated, 12 mL) were used as a color reagent. 2-mL color reagent was added into 2-mL of diluted electrolyte. After 30 min, the absorbance was measured at a wavelength of 458 nm. The standard hydrazine monohydrate solutions with the given concentrations of hydrazine in 0.05 M H_2SO_4 were also prepared for building the calibration curves.

Colorimetric detection of NO_2^-

0.10-mL acidic solution containing 2 M HCl and 10 mg/mL sulfanilamide was dropped into 5 mL of standard or the diluted electrolyte in the test tubes. Subsequently, 0.10-mL N-(1-Naphthyl) ethylenediamine dihydrochloride solution (10 mg/mL) was dropped into the solution. After 30 min, the absorbance of NO_2^- was achieved between 600 nm and 450 nm. The final absorbance of NO_3^- was obtained at 540 nm. The standard calibration curve can be also obtained with the given concentrations of $NaNO_2$.

Faradaic efficiency and ammonia yield rate

FEs and area-normalized yield rates of NH_3, NO_2^-, and N_2H_4 were calculated:

$$\text{FE } (NH_3) = (8F \times C \times V \times n) / Q$$

$$\text{Yield rate } (NH_3) = (17C \times V \times n) / (t \times A)$$

$$\text{FE } (NO_2^-) = (2F \times C \times V \times n) / Q$$

$$\text{Yield rate } (NO_2^-) = (46C \times V \times n) / (t \times A)$$

$$\text{FE } (N_2H_4) = (7F \times C \times V \times n) / Q$$

$$\text{Yield rate } (N_2H_4) = (32C \times V \times n) / (t \times A)$$

Where F is the Faraday constant (96485 C/mol), C is the measured NH_3 concentration, V is the volume of electrolyte, Q is the total charge passed through the electrode, n is the dilution factor and A is the geometer area of the working electrode (1×1 cm^2).

S2. Figures and tables

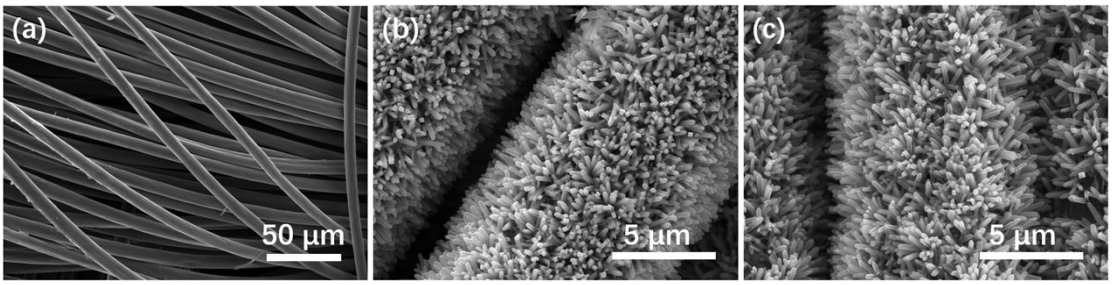

Figure S1. SEM images of the pristine CC (a), TiO_2 (b), and Pd/TiO_2 nanoarrays (c).

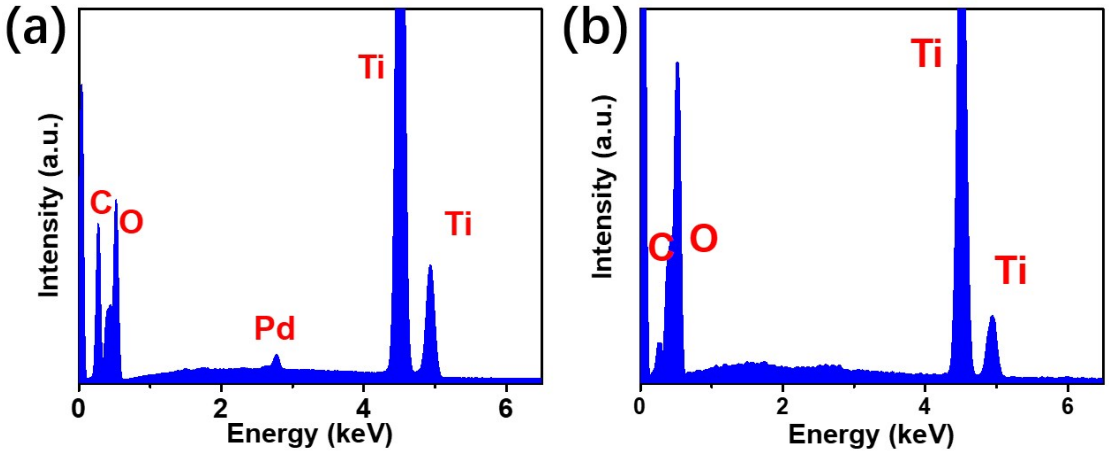

Figure S2. EDX spectra for Pd/TiO_2 nanoarrays (a) and TiO_2 nanoarrays (b).

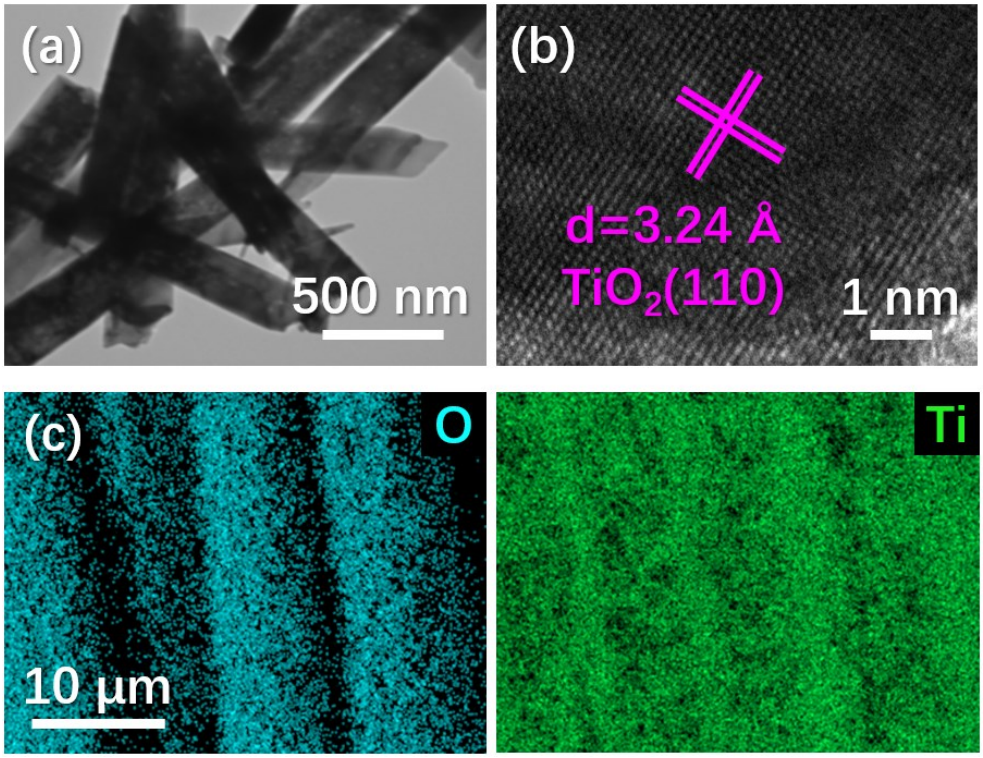

Figure S3. TEM images (a-b) and EDX elemental mapping of TiO_2 nanoarrays.

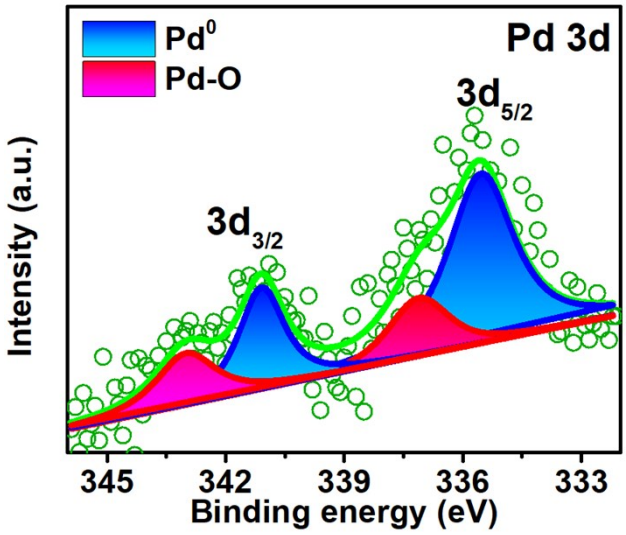

Figure S4. The high-resolution Pd 3 XPS spectrum of the Pd/TiO_2 nanoarrays.

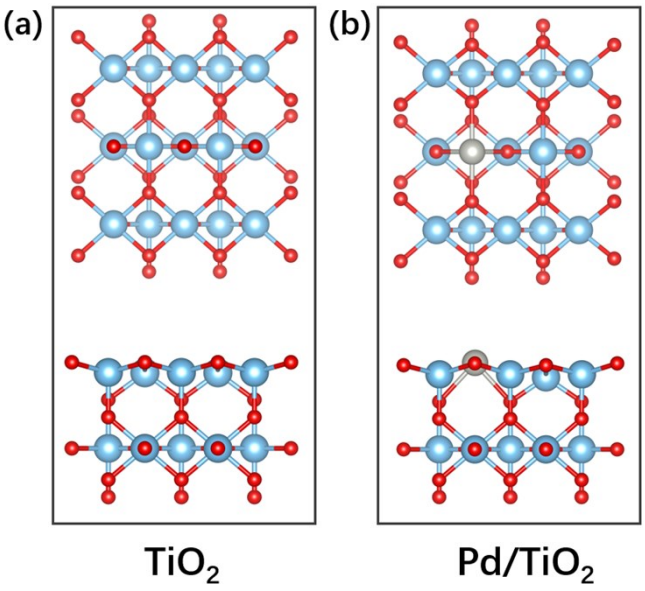

Figure S5. The optimized structures for (a) TiO_2 and (b) Pd/TiO_2.

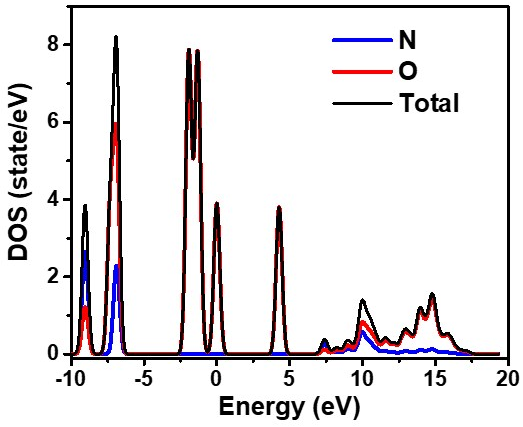

Figure S6. DOS of the free NO_3^-.

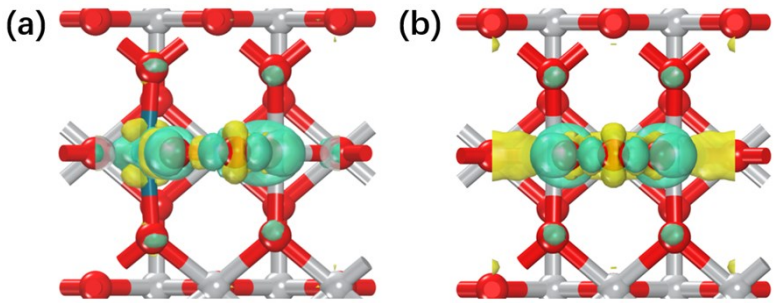

Figure S7. Top views of electron density difference mappings for the optimized Pd/TiO_2-NO_3^- (a) and TiO_2-NO_3^- (b) structures.

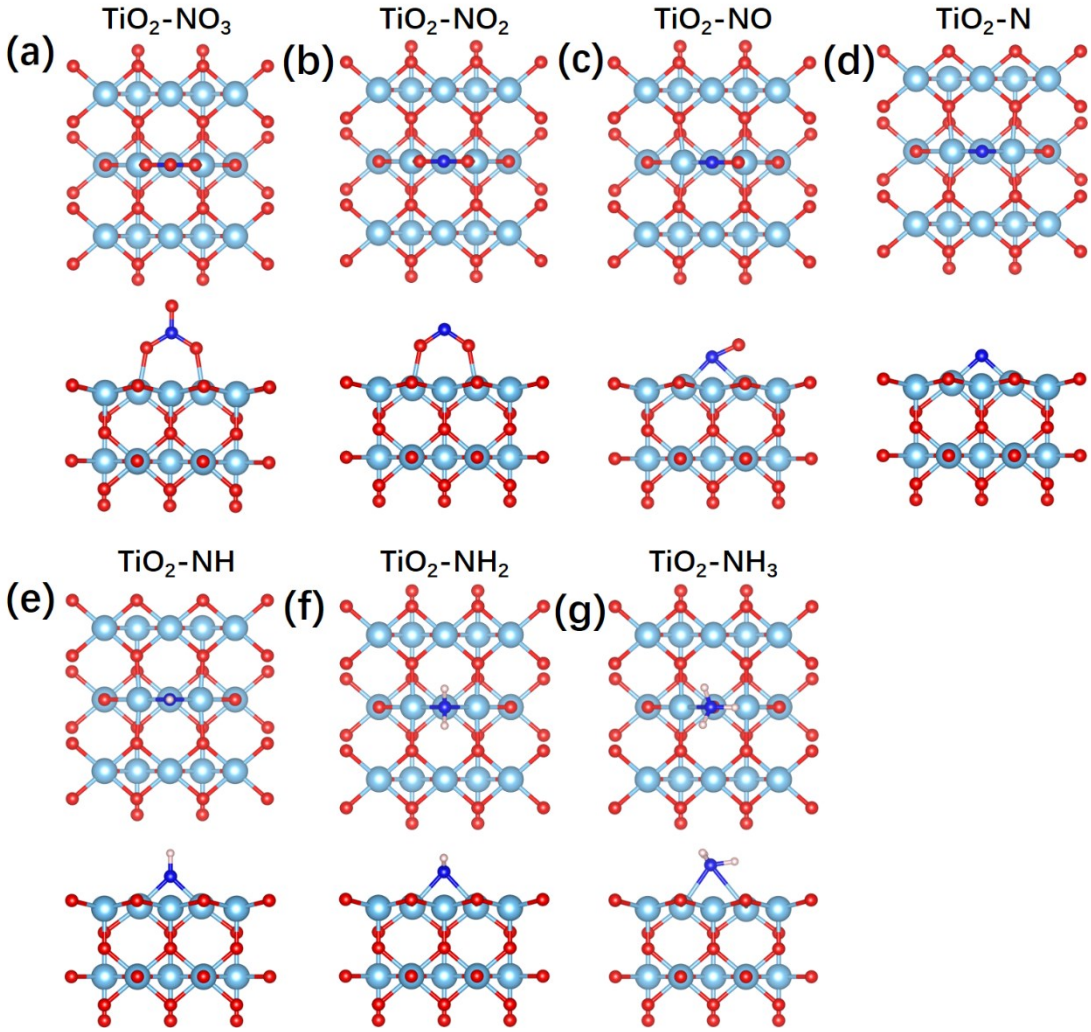

Figure S8. Stable configurations of the intermediates on TiO_2. The most stable adsorption configurations of *NO_3, *NO_2, *NO, *N, *NH, *NH_2, and *NH_3.

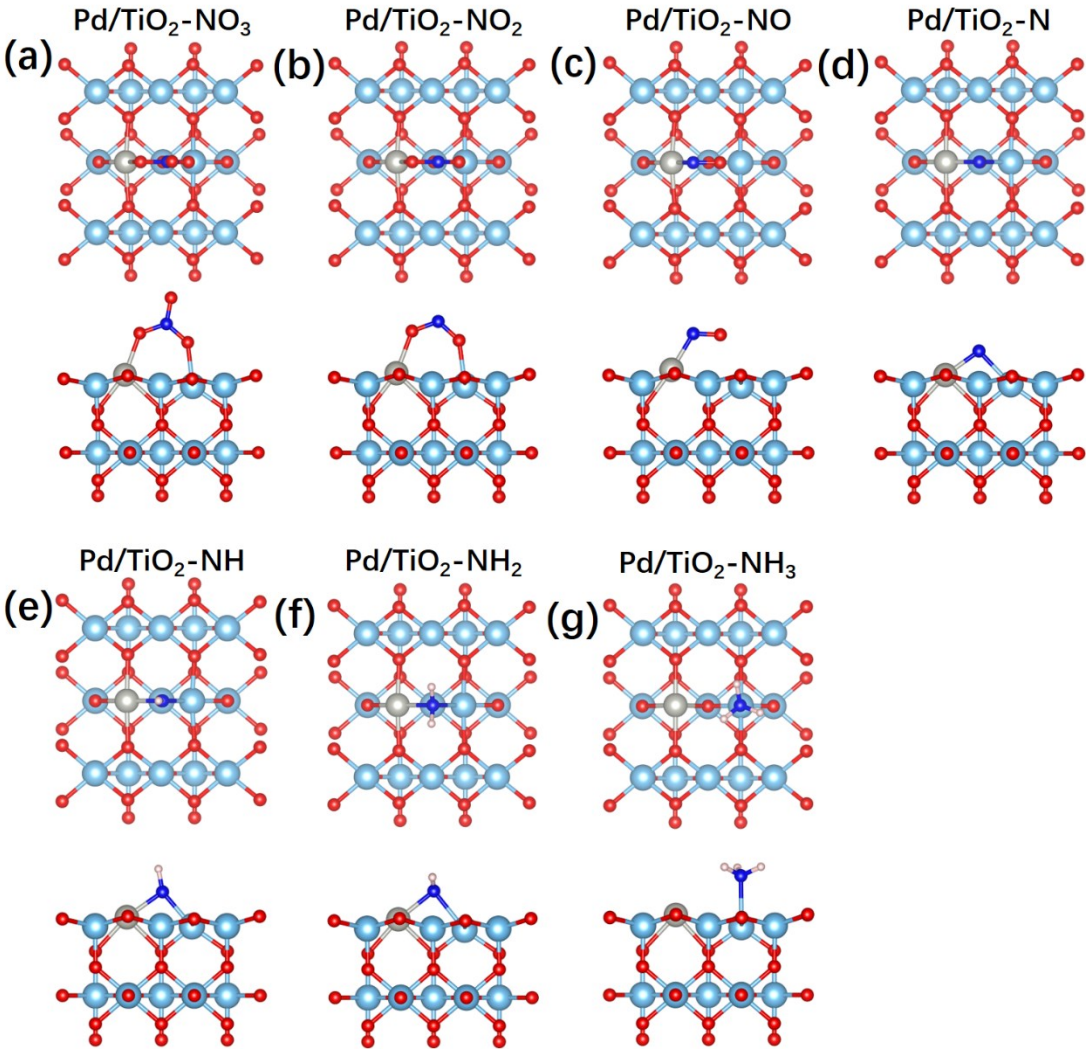

Figure S9. Stable configurations of the intermediates on Pd/TiO_2. The most stable adsorption configurations of $*NO_3$, $*NO_2$, *NO, *N, *NH, $*NH_2$, and $*NH_3$.

As presented in Figures S8-S9, we adopted a side-on adsorption model for NO_3^- on the surfaces of TiO_2 and Pd/TiO_2 based on previous works (*J. Am. Chem. Soc.*, 2020, **142**, 5702-5708, *ACS Catal.*, 2019, **9**, 7052-7064.), where two Ti atoms or a Pd atom and a Ti atom cooperatively act as the active sites for adsorbing NO_3^- and proceeding to the subsequent elemental reactions. Pd and Ti atoms in Pd/TiO_2 synergistically promote the NORR process.

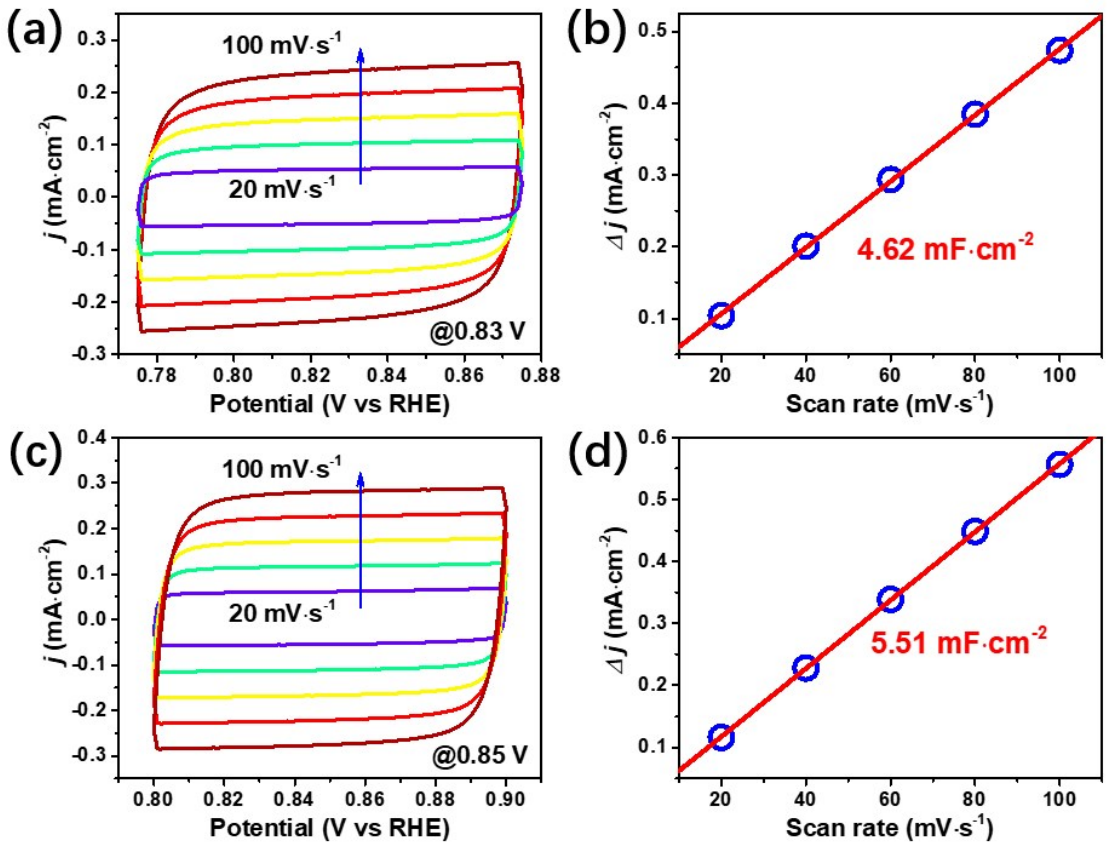

Figure S10. (a, c) The cyclic voltammetry profiles obtained on the pristine TiO_2 and the Pd/TiO_2 nanoarrays at the sweep rates of 20, 40, 60, 80 and 100 mV s^{-1}. (b, d) The determination of double layer capacitance for each catalyst.

The ECSA is estimated from the electrochemical double-layer capacitance of the catalytic surface. The double layer capacitance (*C*dl) has been calculated based on the plot of current density against scan rate. ECSA of working electrode can be calculated according to the equation:

$$\text{ECSA}=R_f \times S$$

where S is generally equal to the geometric area of electrode (in this work, S = 1 cm^{-2}). R_f is the roughness factor of working electrode and determined by the relation:

$$R_f = C\text{dl}/40\ \mu\text{F cm}^{-2}$$

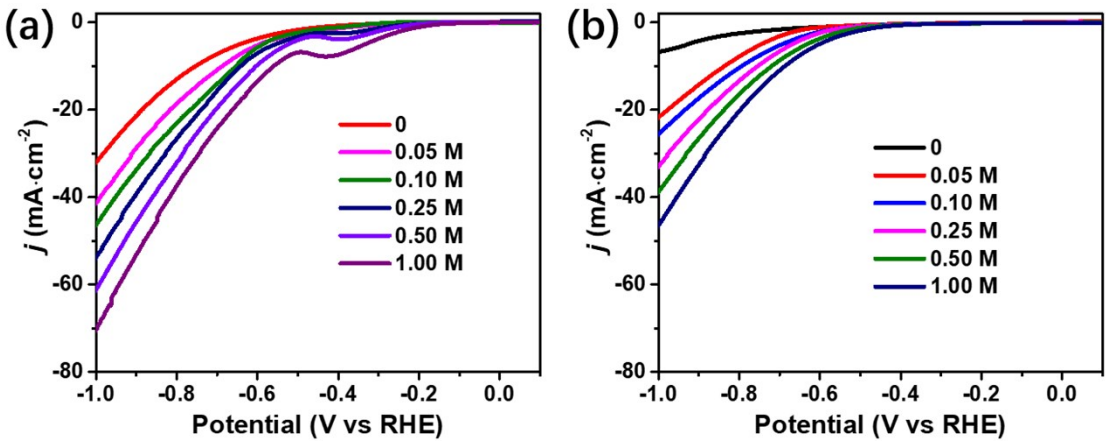

Figure S11. LSV curves over the Pd/TiO_2 nanoarrays (a) and the TiO_2 nanoarrays (b) obtained in 1 M LiCl electrolyte with different $LiNO_3$ that exhibit that both catalysts present the gradual increased current density as the $LiNO_3$ concentration increases in 1 M LiCl electrolyte. Pd/TiO_2 delivers a much larger current density in the electrolyte with an identical concentration of NO_3^- than that of TiO_2. This demonstrates Pd/TiO_2 has the superior capacity of the NORR to TiO_2.

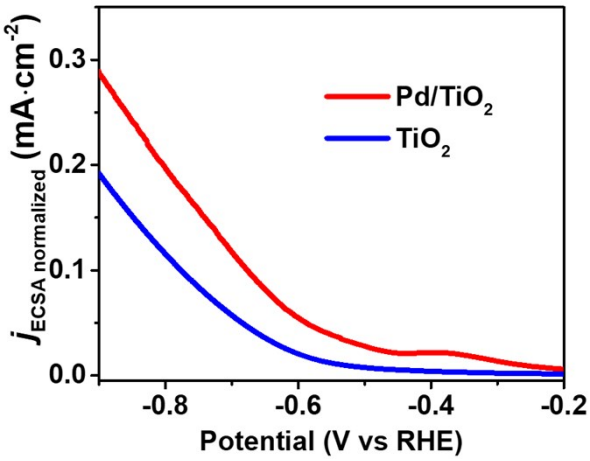

Figure S12. ECSA-normalized current densities for TiO_2 and Pd/TiO_2.

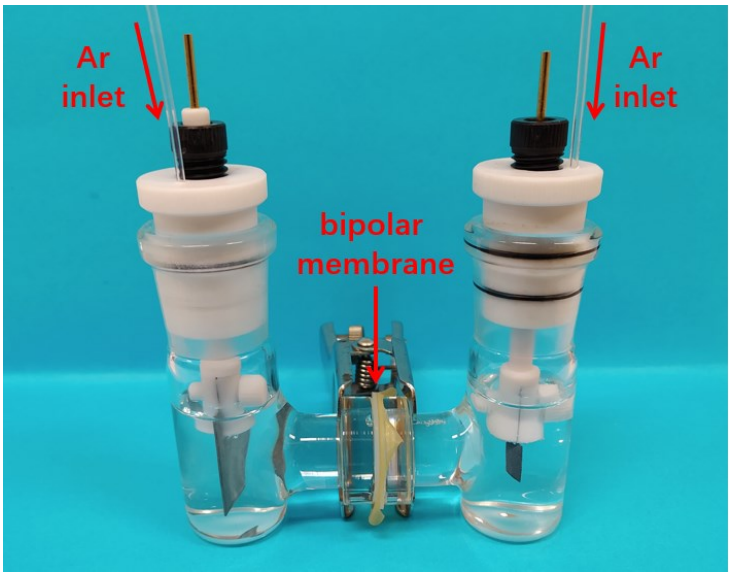

Figure S13. The photograph of the zinc-nitrate battery.

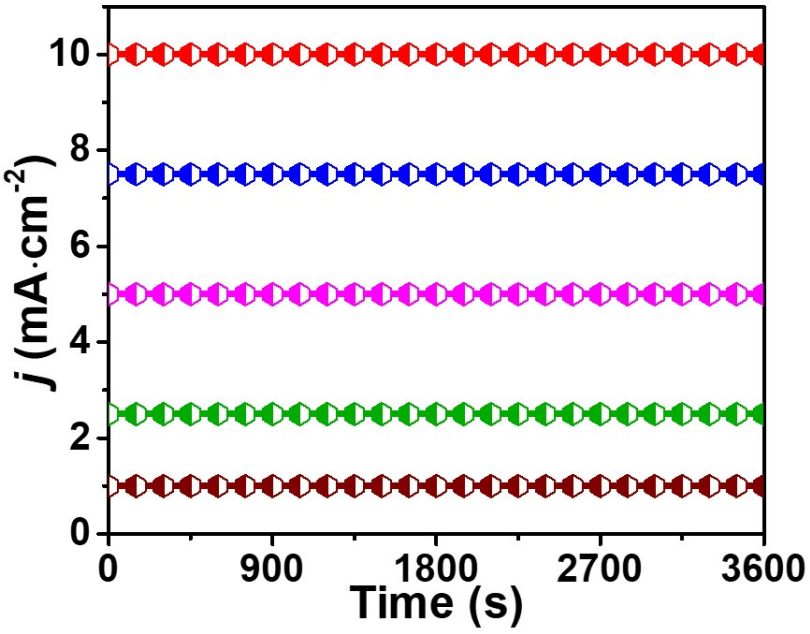

Figure S14. *j-t* curves of the NORR with a Zn-nitrate battery system at different current densities.

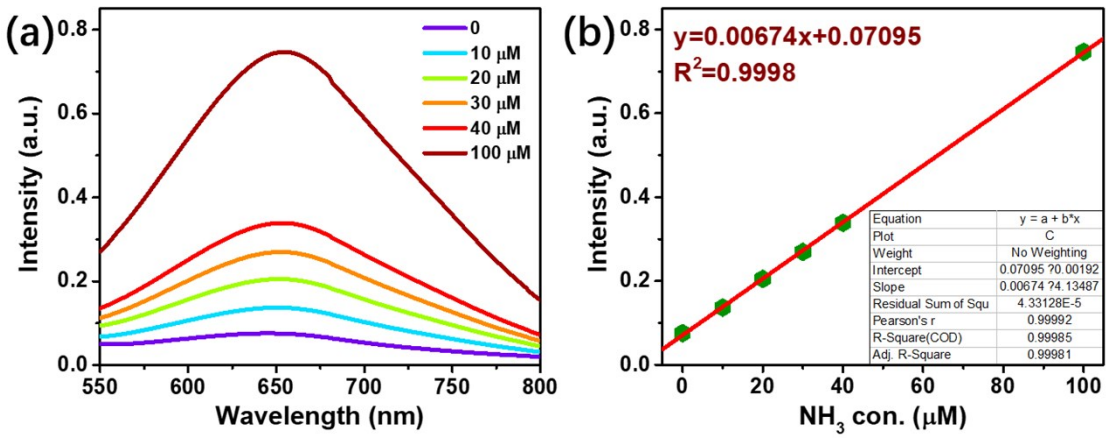

Figure S15. The UV-Vis curves and calibration curves of the electrolyte with the given NH_3 concentrations.

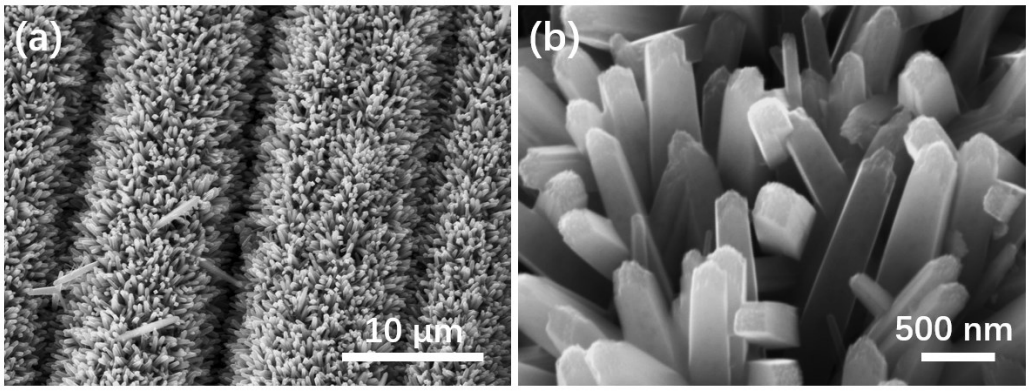

Figure S16. SEM images of Pd/TiO_2 after a 12-h long-term stability test with a Zn-nitrate battery.

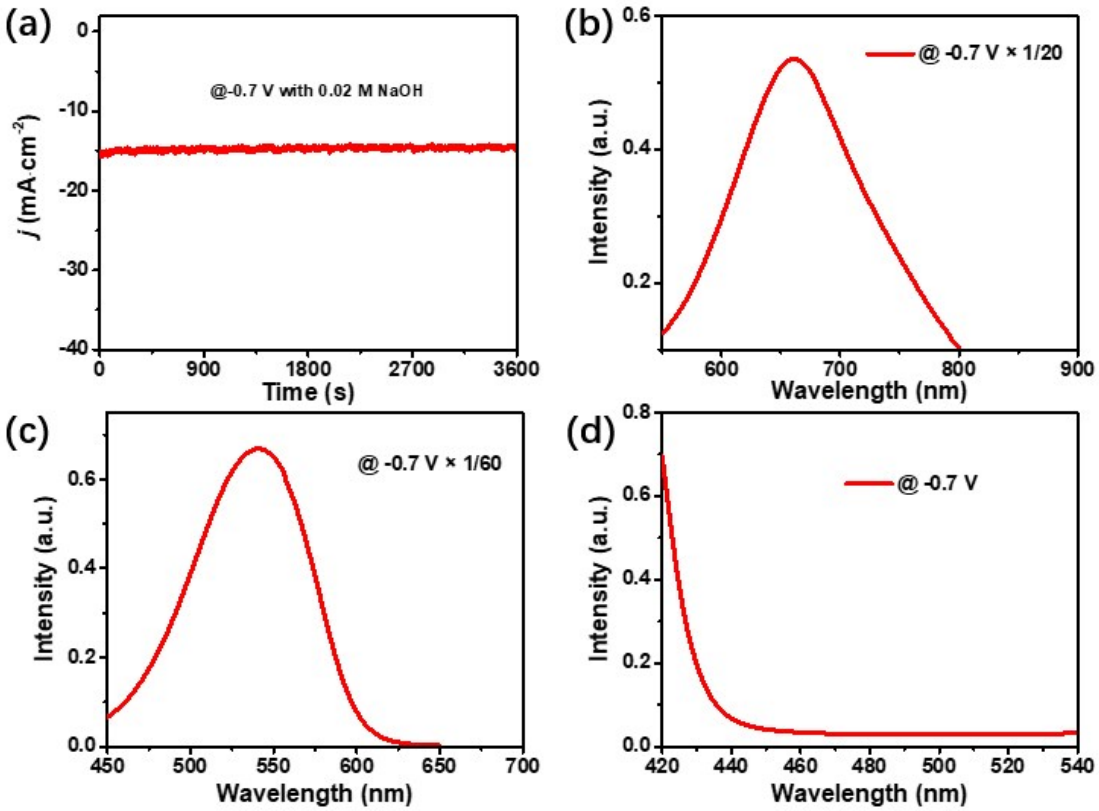

Figure S17. CA curves (a) and (b-d) UV-Vis curves of the Pd/TiO_2 array electrode achieved in the electrolyte with 0.02 M NaOH, (b) NH_3, (c) NO_2^-, and (d) hydrazine.

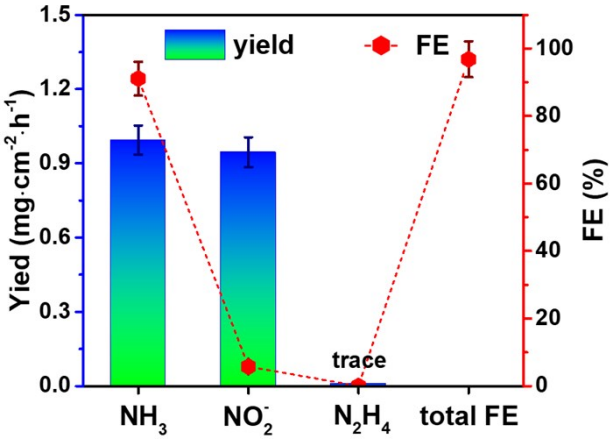

Figure S18. Yields and FEs of the Pd/TiO_2 array electrode achieved in the electrolyte with 0.02 M NaOH.

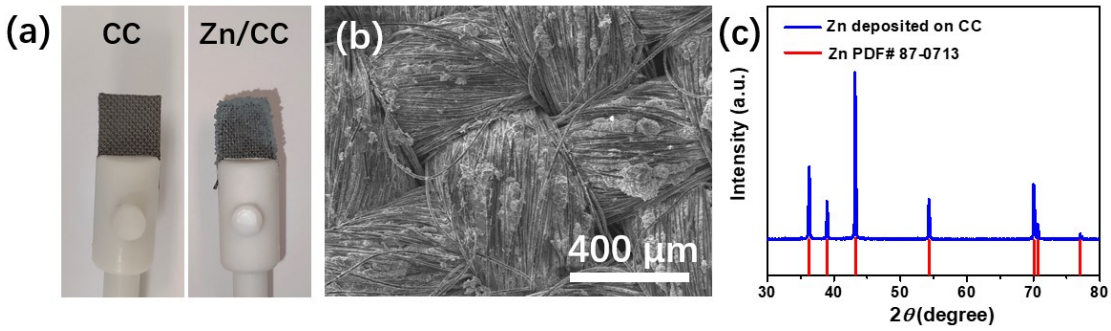

Figure S19. (a) Photographs of the pristine CC and the recycled Zn on CC. (b) SEM image and (c) XRD pattern of the recycled Zn on CC.

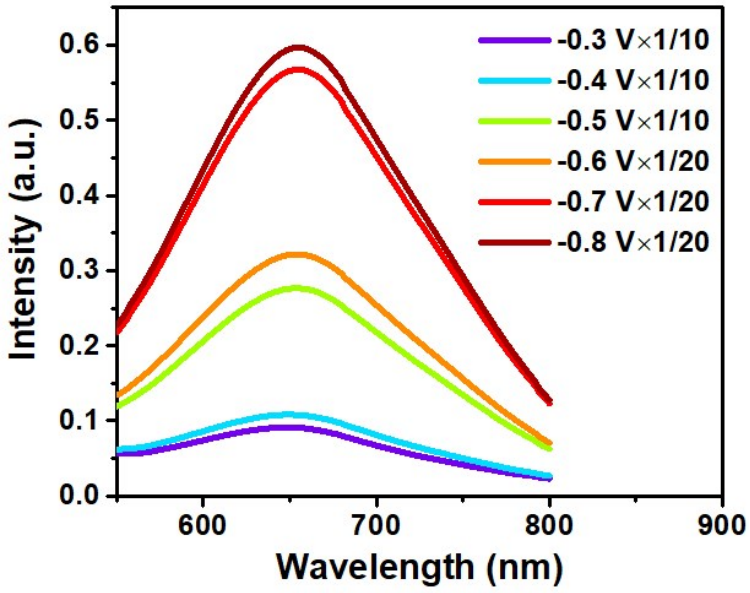

Figure S20. UV-Vis curves of the Pd/TiO_2 catalyst against various work potentials obtained in NO_3^- electrolyte after the NORR test.

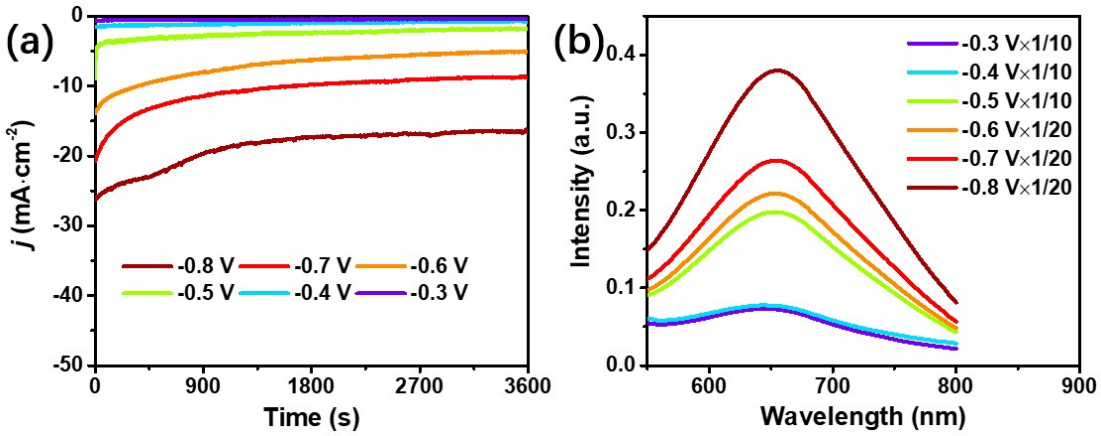

Figure S21. CA curves and UV-Vis curves of the TiO_2 catalyst against various work potentials obtained in NO_3^- electrolyte after the NORR test.

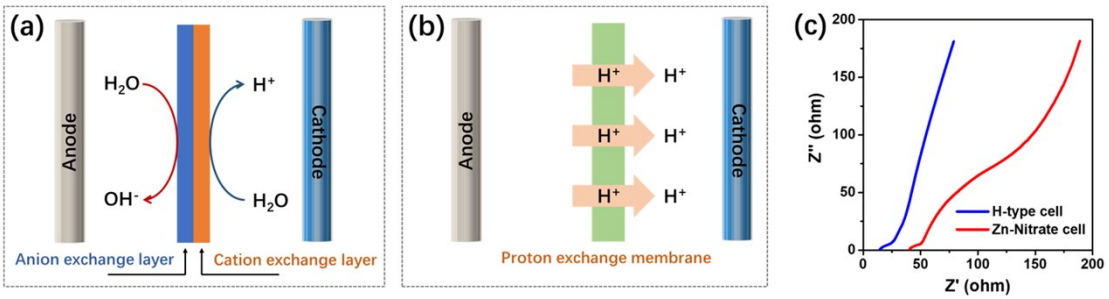

Figure S22. (a-b) Schematic illustrations for the bipolar membrane (a) and the proton exchange membrane (b). (c) EIS plots achieved in two difference cell configurations.

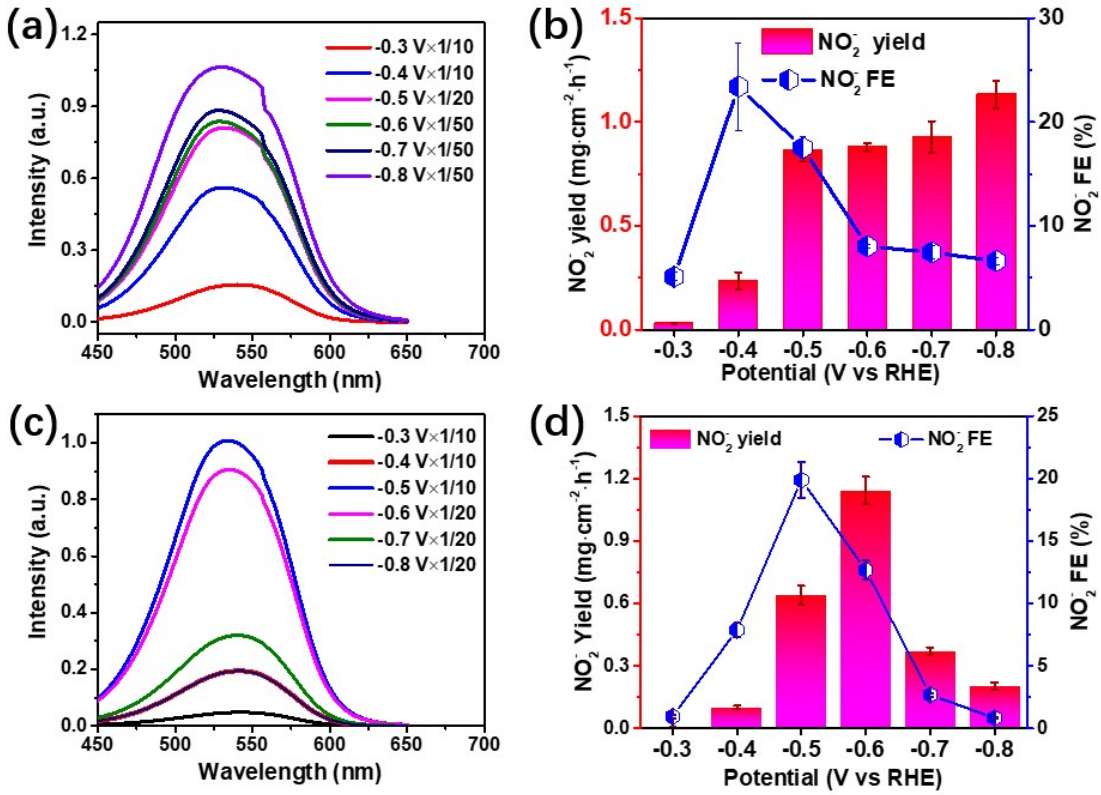

Figure S23. UV-Vis curves and NO_2^- yield and FEs of the Pd/TiO_2 nanoarrays (a-b) and the TiO_2 nanoarrays (c-d) against various work potentials obtained in 1 M LiCl + 0.25 M $LiNO_3$ electrolyte.

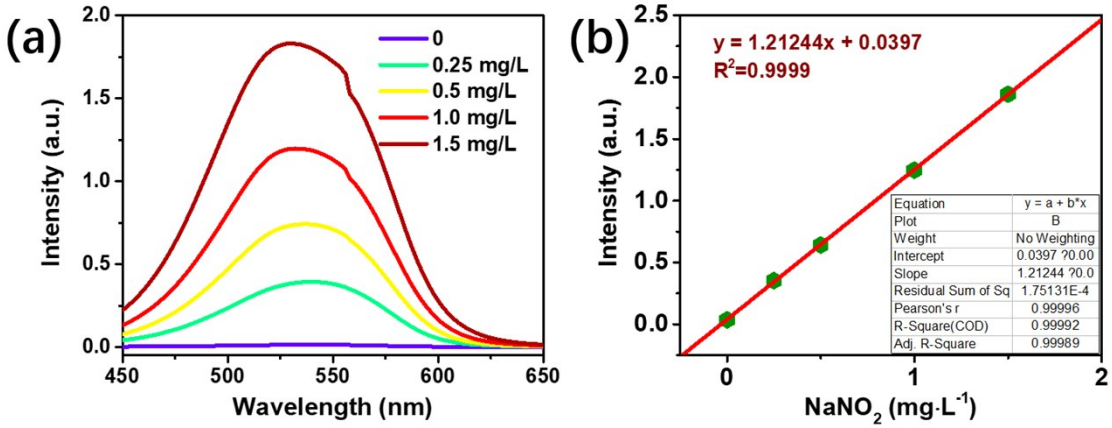

Figure S24. The UV-Vis curves and calibration curves of the electrolyte with the given NO_3^- concentrations.

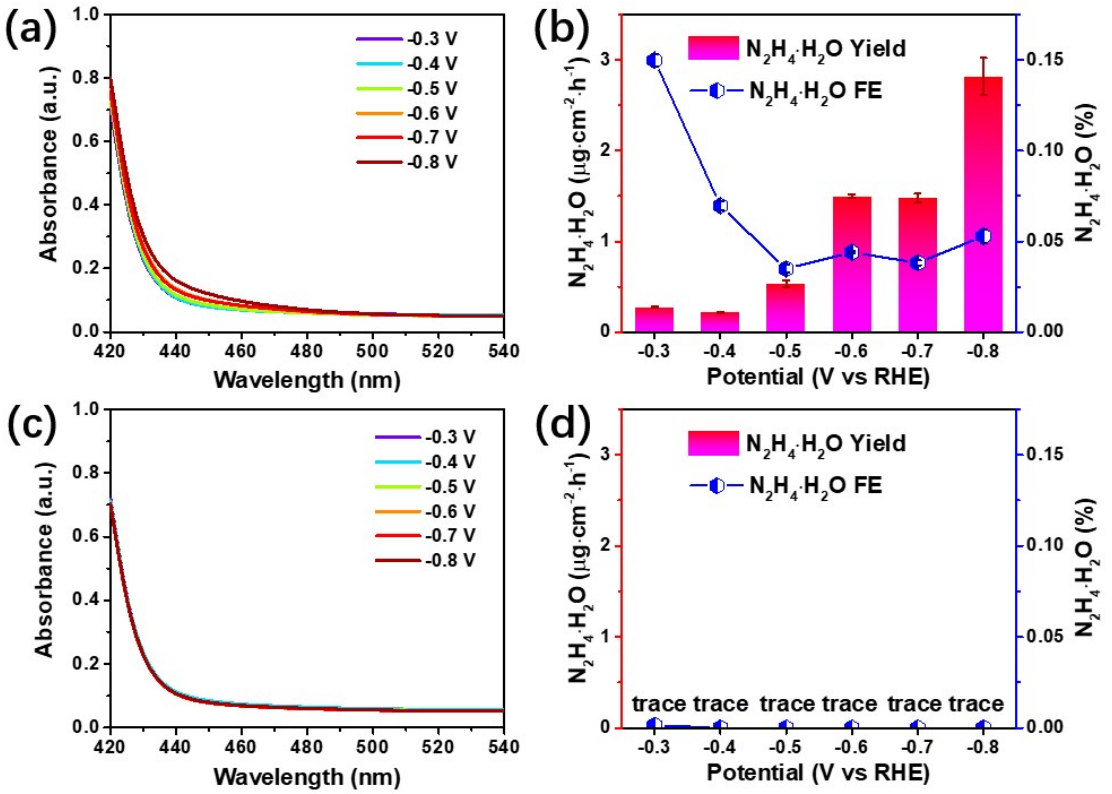

Figure S25. UV-Vis curves and hydrazine yield and FEs of the Pd/TiO_2 nanoarrays (a-b) and the TiO_2 nanoarrays (c-d) against various work potentials obtained in 1 M LiCl + 0.25 M $LiNO_3$ electrolyte.

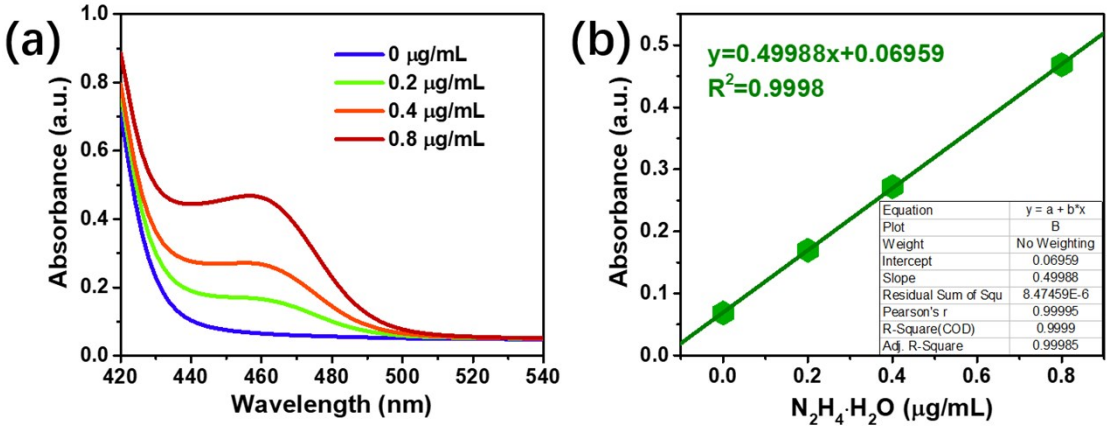

Figure S26. The UV-Vis curves and calibration curves of the electrolyte with the given hydrazine concentrations.

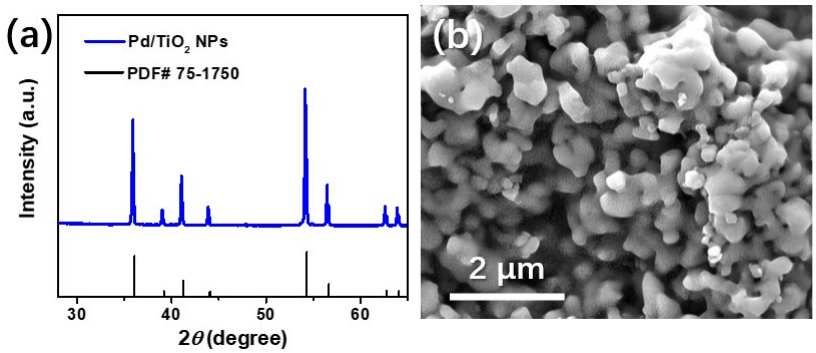

Figure S27. (a) XRD pattern and (b) SEM images of Pd/TiO_2 NPs.

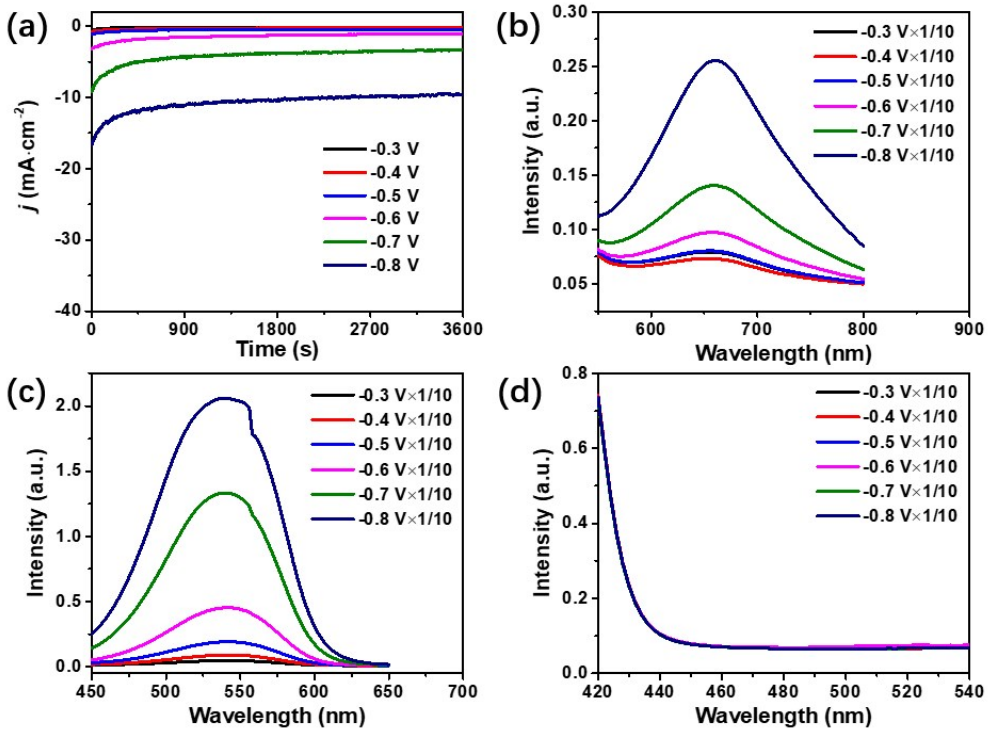

Figure S28. CA curves (a) and (b-d) UV-Vis curves of the Pd/TiO_2 NPs catalyst against various work potentials obtained in NO_3^- electrolyte after the NORR test, (b) NH_3, (c) NO_2^- and (d) hydrazine.

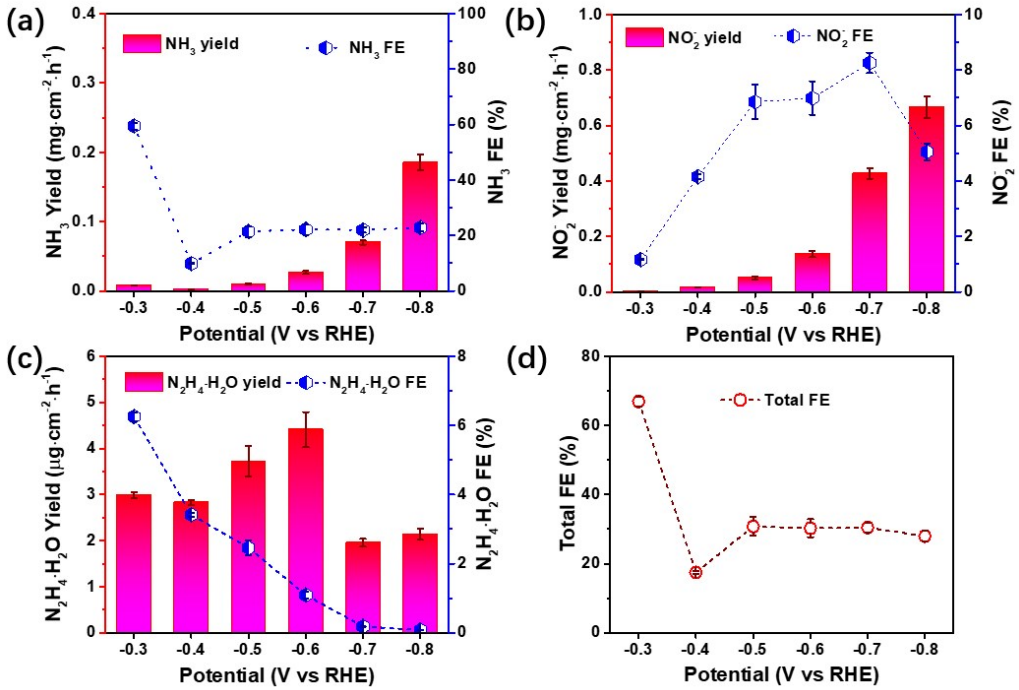

Figure S29. (a-c) yields and FE of the Pd/TiO_2 NPs catalyst against various work potentials, (a) NH_3, (b) NO_2^-, and (c) hydrazine. (d) Total FE of the Pd/TiO_2 NPs catalyst achieved at different potentials.

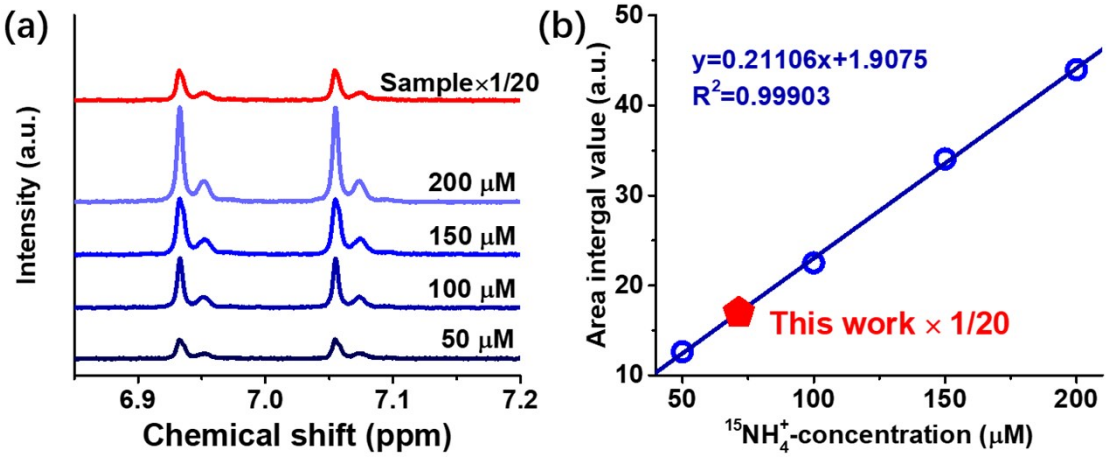

Figure S30. (a) ^{1}H NMR spectra of the electrolyte and $(^{15}NH_4)_2SO_4$ reference with the given concentrations. (b) The corresponding calibration curve from ^{1}H NMR spectra.

Table S1. The theoretical data for several types of metal-based batteries.

Battery type	Chemical reaction	Theoretical Voltage (V)	Theoretical Capacity* ($mAh\ g^{-1}$)	Energy Density* ($Wh\ kg^{-1}$)
Li-S	$2\ Li + S = Li_2S$	2.2	1167	2566
Li-O_2	$2\ Li + O_2 = Li_2O_2$	3.0	1168	3504
Li-CO_2	$4\ Li + 3CO_2 = C + 2\ Li_2CO_3$	2.7	67	1809
Li-N_2	$6\ Li + N_2 = 2\ Li_3N$	0.54	2311	1248
Zn-CO_2	$Zn + CO_2 + H_2O = ZnO + HCOOH$	0.955	421	402
Al-N_2	$2Al + N_2 = 2AlN$	0.99	1961	1941
Zn-Air	$2\ Zn + O_2 = 2\ ZnO^-$	1.65	670	1105
Zn-nitrate	$4Zn + NO_3^- + 3H_2O \rightarrow 4ZnO + NH_4OH + OH^-$	1.85	568	1051

*This calculated value is based on the reaction products of the battery reaction equation.

Table S2. Performance comparison of the well-developed catalysts for NORR and NRR.

	Catalyst	NH_3 FE (%)	NH_3 Yield (mg□cm^{-2} h^{-1})	Reference
Electro-reduction of nitrate into ammonia	**Pd/TiO_2**	**92.05**	**1.12**	**This work**
	PTCDA/O-Cu	77	0.436	S1
	TiO_{2-x}	85	0.765	S2
	Cu/Cu_2O NWAs	81.2	0.1633	S3
	Ti/RuO_2	52.1	0.271	S4
	Cu/Ni	76.5	0.35	S5
	Fe^0/Fe_3O_4	32	0.0775	S6
	Co_3O_4/Ti	80	0.634	S7
	ZVT sheets	6	0.0588	S8
Electro-reduction of N_2 into ammonia	Pd_3Cu_1	1.22	0.0399	S9
	Fe/TiO_2	25.6	0.02547	S10
	$Bi\text{-}TiO_2$	17.3	0.0089	S11
	PdPb	5.79	0.02568	S12
	TiO_2/rGO	3.3	0.01513	S13
	Pd/C	8.2	0.0045	S14
	PdO/Pd	11.5	0.0182	S15
	PdH	43.6	0.0204	S16
	$V\text{-}TiO_2$	15.3	0.01773	S17
	PdRu	1.53	0.02592	S18
	$TiO_2(V_O)$	6.5	0.003	S19

S3. Reference

S1. Nature Energy **2020**, 5, 605-613.

S2. ACS Catal. **2020**, 10, 6, 3533–3540.

S3. Angew. Chem. Int. Ed. **2020**, *59*, 5350.

S4. Catal. Lett. **2019**, 149, 1216–1223.

S5. Electrochimica Acta **2018**, 291, 151-160.

S6. J. Clean. Prod. **2020**, 242, 118569.

S7. Appl.Catal. B-Environ. **2019**, 254, 391-402.

S8. Water Res. **2019**, 157, 191-200.

S9. Nano Energy 2019, 58, 834.

S10. Angew. Chem. Int. Ed.2019, 58, 18449-18455.

S11. Nature Commun. 2019, 10,2877.

S12. Appl.Catal. B-Environ. *2020, 265*, 118481.

S13. J. Mater. Chem. A, 2018, 6, 17303

S14. Nat. Commun. *2018, 9*, 1795.

S15. J. Mater. Chem. A, 2019, 7, 12627.

S16. Angew. Chem. Int. Ed. 2020, 59, 3511-3516.

S17. Small Methods 2019, 1900356.

S18. ACS Sustainable Chem. Eng. 2019, 7, 2400.

S19. Appl. Catal. B-Environ. 2019, 257,117896.